Nanoscale

Cite this: *Nanoscale*, 2012, **4**, 4680

www.rsc.org/nanoscale

PAPER

Multi-photon imaging of amine-functionalized silica nanoparticles†

Filipe Natalio,[a] Anubha Kashyap,[b] Steffen Lorenz,[b] Hannes Kerschbaumer,[a] Michael Dietzsch,[a] Muhammad Nawaz Tahir,[a] Heinz Duschner,[c] Susanne Strand,[b] Dennis Strand[b] and Wolfgang Tremel*[a]

Received 19th March 2012, Accepted 17th April 2012
DOI: 10.1039/c2nr30660c

A convenient and simple strategy for preparing water soluble, photoluminescent functionalized silica nanoparticles (M-dots) in the absence of fluorophores or metal doping is demonstrated. These M-dots can be used for bioimaging using one and two-photon microscopy. Because of their high photostability, low toxicity and high biocompatibility compared with Lumidot™ CdSe/ZnS quantum dots, functionalized silica particles are superior alternatives for current bioimaging platforms. Moreover, the presence of a free amine group at the surface of the M-dots allows biomolecule conjugation (*e.g.* with antibodies, proteins) in a single step for converting these photoluminescent SiO_2 nanoparticles into multifunctional efficient vehicles for theragnostics.

Introduction

Fluorescence microscopy has become increasingly popular during the past few decades because it provides the ability to selectively distinguish small biological structures at the cellular, sub-cellular, and molecular levels.[1,2] Most fluorescence imaging techniques rely on endogenous or exogenous fluorophores that are excited with UV radiation.[3–5] Further advances in live imaging techniques have been achieved with the invention of two- and multi-photon fluorescence microscopy.[6–9]

Multi-photon microscopy possesses some advantages over conventional confocal microscopy, such as reduced fluorescence background because of the relatively low two-photon cross-section of most biomolecules responsible for autofluorescence, reduction of photobleaching by selective excitation of the focal volume, and improved depth penetration in scattering samples by using excitation radiation within the optical transmission window of biological tissues (near-infrared (NIR) spectral range, 700–1000 nm).[10]

Among the best performing two-photon fluorescence materials are quantum dots (QDs)[11–13] and metallic nanoparticles.[14,15] However, there is much concern about the toxicity of the heavy metal components used,[16–19] and the two-photon emission spectra of gold nanoparticles strongly depend on their shape and environment.[20] More recently, carbon dots,[21] silicon[22] or lanthanide (Ln^{3+}) doped nanoparticles,[23,24] in particular $NaLnF_4$ doped with erbium (Er^{3+}), ytterbium (Yb^{3+}) and thulium (Tm^{3+}) have emerged as alternatives to quantum dots and metal nanoparticles. Still, the search for stable and non-toxic alternatives remains an important task to be addressed.

Dye-free luminescent silica without metal activators is a promising "green" phosphor that can be obtained by condensation of alkoxysilanes in the presence of organic acids.[25] A recent modification of the original procedure[26,27] led to the formation of nearly monodisperse luminescent silica spheres. Alternative routes to dye- and metal-free luminescent silica nanoparticles have been reported.[28,29] The emergence of these photoluminescent silica nanomaterials offers exciting opportunities in the search for stable and non-toxic fluorophores that are highly desired in bio-imaging, disease detection, and drug delivery.[30,31]

Here we report that photoluminescent amorphous silica nanoparticles (M-dots) (~13 nm) can be prepared, in the absence of fluorophores or metal doping, *via* a novel low-temperature wet-chemical methodology of surface-functionalization, thereby overcoming laborious multistep procedures of nanoparticle functionalization. The acquired intrinsic photoluminescence seems to be related to the formation of an amorphous silicon oxynitride (SiO_3–N) surface layer. The presence of an amine moiety at their surface renders the M-dots easily dispersible in aqueous environments; thus they can easily be conjugated with a wide range of biomolecules *via* amide bonds. Compared with fluorescent semiconductor nanocrystals (*e.g.* CdSe/ZnS quantum dots – QDs – Lumidot™), the M-dots show superior chemical inertness and biocompatibility with dendritic cells (DCs), *i.e.* they exhibit significantly lower toxicity. In addition, the M-dots are not only one-photon active, displaying high photostability

[a]*Institut für Anorganische Chemie und Analytische Chemie, Johannes Gutenberg-Universität, Duesbergweg 10-14, 55099 Mainz, Germany. E-mail: tremel@uni-mainz.de; Fax: +49-6131-39-25605; Tel: +49-6131-39-25135*
[b]*Medizinische Klinik, Universitätsmedizin der Johannes Gutenberg-Universität, Langenbeckstrasse 1, 55131 Mainz, Germany*
[c]*Angewandte Struktur- und Mikroanalytik, Universitätsmedizin der Johannes Gutenberg-Universität, Obere Zahlbacher Str. 6, 55131 Mainz, Germany*

† Electronic supplementary information (ESI) available: TEM images of unfunctionalized, XRD, UV-Vis spectra, XPS spectra and gallery of two-photon images. See DOI: 10.1039/c2nr30660c

and low blinking, but also are two-photon active. Here we show the synthesis of biocompatible photoluminescent SiO_2 nanoparticles (M-dots) using a simple synthetic functionalization method that allows a facile conjugation of biomolecules and represents an alternative to current nano-platforms (*e.g.* QDs) for biomedical/bioimaging applications.

Methods and materials

SiO_2 nanoparticle functionalization

Amorphous silica nanoparticles (cat. no. 420883, Ludox® colloidal silica suspension in water, Sigma, Germany) were surface chlorinated with $SOCl_2$ using a modified protocol from ref. 32. Briefly, 20 mL of $SOCl_2$ (cat. no. 230464, ReagentPlus®, ≥99.0%, Sigma, Germany) and 1 mL of anhydrous DMF (cat. no. 227056, >99.9%, extra dry, Sigma, Germany) were added to 100 mg of silica nanoparticles and reacted at 70 °C for 24 h. Afterwards the product was cooled to room temperature and centrifuged (9000× rpm, 15 min, RT). The yellow supernatant was discarded and the Cl functionalized nanoparticles were washed twice with anhydrous THF (cat. no. 401757, anhydrous, ≥99.9%, inhibitor-free, Sigma, Germany) using a centrifugation step (9000× rpm, 15 min, RT). Subsequently, Cl-functionalized SiO_2 nanoparticles were further functionalized with *N*-Boc-1,4-butanediamine. For this purpose, *N*-Boc-1,4-butanediamine (0.5 g) (cat. no. 15404, purum, ≥97.0%, Sigma, Germany) was added to Cl-functionalized SiO_2 nanoparticles (100 mg) and reacted for 96 h at 85 °C under continuous stirring. The solution was cooled to RT and extensively washed with pure ethanol using a centrifugation step (9000× rpm, 15 min, RT). The BOC-amine end was deprotected by reacting the functionalized nanoparticles with HCl (0.1 M) in pure methanol (1 h, RT).[33] The samples were brought to dryness under vacuum.

Physical characterization of SiO_2 based nanoparticles

The nanoparticles were characterized by means of transmission electron microscopy (TEM), dynamic light scattering (DLS), zeta potential (ξ) and CP MAS ^{29}Si-NMR. For transmission electron microscopy (TEM) the samples were loaded onto copper grids coated with carbon (Plano, Wetzlar; Germany) and morphologically characterized using TEM (Philips 420 instrument) with an acceleration voltage of 120 kV. Dynamic light scattering (DLS) experiments were performed at an ALV-7004 correlator setup, equipped with an ALV/CGS-8FDLS/SLS 5022F goniometer, an ALV 7004 correlator and a QEAPD avalanche photodiode detector. A He–Ne-laser ($\lambda = 632.8$ nm, $P = 200$ mW) served as a coherent light source. Measurements were carried out at $T = 293$ K and at angles of $\theta = 30, 47, 64, 81, 98, 115, 132$ and 149°. The samples were filtered (0.5 μm) prior measurements. Zeta potential (ξ) measurements were performed in triplicate on a Malvern Zetasizer Nano ZS. Infrared analysis was performed using a Nicolet Nexus spectrometer fitted with a Golden Gate attenuated total reflection (ATR) accessory (Thermo Nicolet). Spectra were recorded at 4 cm^{-1} resolution, averaging 32 scans. The ^{29}Si-NMR spectra were obtained on a Bruker DSX 400 Avance NMR spectrometer equipped with the CP MAS probe (Bruker Analytik, Karlsruhe, Germany) at resonance frequency of 400 MHz with 4.0 mm CP/MAS probe head and operating at a spinning speed of 5 kHz.

X-ray photoelectron spectroscopy (XPS)

XPS analysis was performed on a PHI 5600 ci X-ray photoelectron spectrometer (Physical Electronics, USA) with a non-monochromatic Al Kα X-ray source (14 kV) operated at 300 W and using a base pressure of 5×10^{-10} mbar. A pass energy of 58.7 eV was used. The spectra were recorded using a 45° take off angle relative to the surface normal. The binding energies were referenced to the C1s line at 284.8 eV from alkyl or adventitious carbon. The XPS scans were analyzed using the Avantage 4.15 software.

Photoluminescence

Fluorescence spectra (emission) were measured in a semi-micro cuvette with a Jobin-Ivon Spex Fluoromax-2 spectrofluorimeter. Fluorescence spectra were corrected for wavelength-dependence of the fluorimeter as well as for the inner filter effect both for excitation and emission.[34] The resulting spectra of amine-functionalized SiO_2 nanoparticles (M-dots) were integrated to obtain a measure of the quantum yield (ϕ).

Ligand exchange of CdSe/ZnS quantum dots (QDs)

Commercially available CdSe/ZnS quantum dots (QDs) (cat. no. 694592, Lumidot™ CdSe/ZnS 480, core–shell type quantum dots, 5 mg mL^{-1} in toluene) surface stabilized with hexadecylamine (HDA) ligand were transferred to an aqueous medium (deionized water) by exchanging the initial ligand with *O*-[2-(3-Mercapto-propionylamino)ethyl]-*O*′-methyl polyethylene glycol – 5000 (SH–PEG–OCH_3) (cat. no. 712523. Aldrich, Germany) to render the QDs water soluble. Typically, 1 mg of QDs were mixed with 2 mg of PEGylated thiol (SH–PEG–OCH_3) in 5 mL of $CHCl_3$. The reaction was allowed to stir for 6 h at RT under argon. Phase transfer of the functionalized QDs into deionized water was achieved by adding 10 mL of hexane and 2 mL of deionized water under vigorous stirring. The aqueous phase containing the QDs was separated with a separating funnel. The (SH–PEG–OCH_3) stabilized QDs were stored at 4 °C under dark conditions.

Cell culture and cytotoxic assay

Human dendritic cells (DCs) were obtained by isolating monocytes from donated Buffy coat. To obtain immature DCs, monocytes were cultured in the presence of 800 IU mL^{-1} of GM-CSF and 1000 IU mL^{-1} of IL-4 in RPMI media for 7 d. To perform the cytotoxic assay, 2×10^4 DCs were cultured in a 96 well plate and M-dots and PEGylated-QDs quantum dots (Lumidot™ core–shell CdSe/ZnS) were added at given concentrations (50, 100 and 200 μg mL^{-1}) in four independent wells. After 18 h at 37 °C/5% CO_2, the cell viability was determined by CellTiter-Glo viability assay kit (Promega, Germany) according to the manufacturer instruction and measured in a SpectraFlour Plus reader (Tecan, Austria). From four wells, the average readings were taken and the percentage survival was calculated for each treatment considering untreated cells as 100%.

Incubation of M-dots and QDs with DCs and imaging

DCs (3×10^4) were plated in Lab-Tek 8-well chamber slides (Thermo Fisher Scientific, Germany) and left for 24 h at 37 °C/5% CO_2. Afterwards, PEGylated-QDs Lumidot™ core–shell CdSe/ZnS and M-dots (50, 100 and 200 μg mL^{-1}) were co-incubated for 24 h at 37 °C/5% CO_2. After washing, the intracellular localization of nanoparticles was confirmed by imaging the cells using confocal laser scanning microscopy CLSM.

Confocal laser scanning microscopy (CLSM)

(a) *One-photon*: microscopic analysis was performed on a CLSM (Zeiss LSM 710 confocal laser scanning microscope equipped with Zen 2009 software, Carl Zeiss, Germany) with $l_{ex} = 408$ nm, adjusted to 4% of 30 mW laser power. For the bleaching experiments, a selected area of the sample was chosen and irradiated with $l_{ex} = 408$ nm, adjusted to 20% of the 30 mW laser power for 120 s, and the intensity decay was recorded. (b) *Two-photon*: two-photon images were obtained on a Zeiss LSM 710 NLO microscope equipped with Non Descanned Detectors (NDDs). For image acquisition a LD C-Apochromat 40×/1.1 W Korr M27 objective was used and the samples were excited at 753 nm using a Chameleon Ultra Ti-Sapphire laser (Coherent). 5% laser power 305 mW was used for imaging while 14% laser power was used for bleaching experiments (for 130 s). The emitted fluorescence was passed through 455–500, 500–550 and 565–610 band pass filters to NDDs. Fluorescence spectra were generated with the 34-channel QUASAR detector. All data were acquired and processed using the Zen 2009 software.

Results and discussions

Transmission electron microscopy (TEM) analysis of the commercially available amorphous SiO_2 nanoparticles (Ludox™) showed an average size of ~13 nm (Fig. S1A and B, ESI†) and a high polydispersity. These SiO_2 nanoparticles (100 mg) were treated with an excess of $SOCl_2$ and DMF for 24 h at 70 °C under anhydrous conditions. This chemical treatment yielded a reactive surface intermediate (SiO_x–Cl $3 > x > 1$) by replacing the surface silanol groups with Cl.[35] After removing excess $SOCl_2$–DMF, the nanoparticles were washed twice with anhydrous THF and treated subsequently with *N*-Boc-1,4-butanediamine (96 h at 85 °C) to specifically couple the free amino group to the SiO_2–Cl nanoparticles through nucleophilic attack of the NH_2 group to the Si activated center.[36] Unbound *N*-Boc-1,4-butanediamine was removed by extensive washing with ethanol. The protecting *N*-Boc groups were removed by reacting the functionalized nanoparticles with HCl (0.1 M) in pure methanol (for 1 h at RT).[33] These functionalized SiO_2 nanoparticles are referred to as M-dots (Fig.1).

The morphology of the M-dots and their successful functionalization (with subsequent Boc deprotection) were analyzed by TEM, FT-IR, DLS, zeta potential (ζ), CP MAS ^{29}Si NMR and XPS techniques respectively. Fig. 2A shows a representative TEM image of the M-dots that, after functionalization, retain their initial size (~13 nm) and morphology but remain partially clustered (significantly less than the initial SiO_2 nanoparticles). The presence of the ligand (after Boc-deprotection) was confirmed by FT-IR analysis (Fig. 2B) where the typical CH_2 and

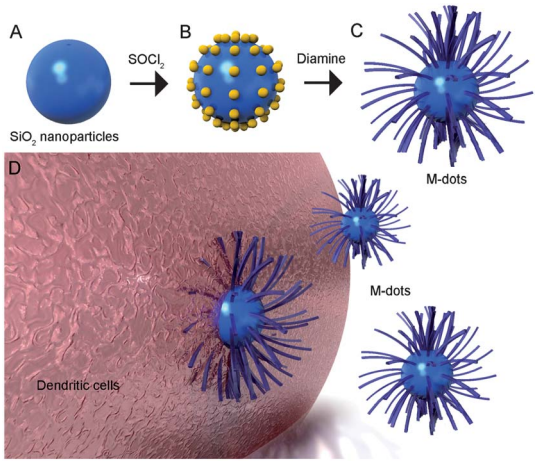

Fig. 1 Schematic representation of (A) SiO_2 nanoparticles, (B) their surface functionalization with $SOCl_2$ and (C) *N*-Boc-1,4-butanediamine. This functionalization displays an intrinsic one- and two-photo-luminescence and high biocompatibility and thus can be used (D) for biomedical applications such as bioimaging, representing a versatile alternative to current technological platforms.

NH_2 (N–H stretching) vibration frequencies were observed at 2975 and 2926 cm^{-1} and 1525 cm^{-1}, respectively (Fig. 2B, red line and inset), not present in the FT-IR spectrum recorded for the unfunctionalized SiO_2 nanoparticles (Fig. 2B, black line). Boc deprotection using this methodology proved extremely convenient as no further laborious work-up was required. DLS

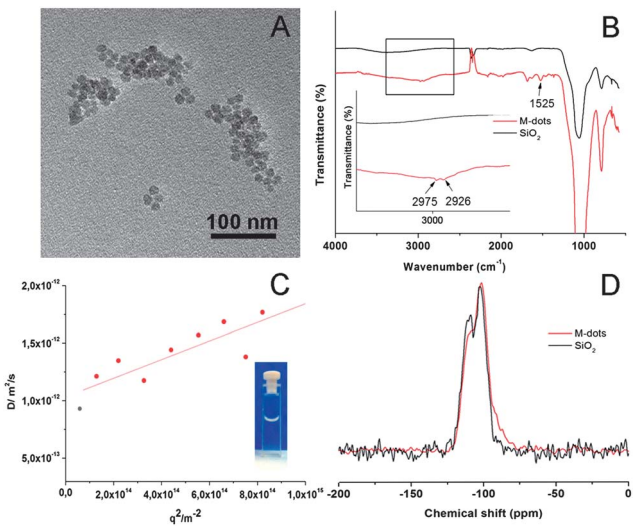

Fig. 2 (A) Transmission electron microscopy (TEM) images of M-dots (SiO_2 nanoparticles functionalized with 1,4-butanediamine) showing that the particle morphology was retained after functionalization. (B) FT-IR spectra of SiO_2 nanoparticles (black line) and functionalized with *N*-Boc-1,4-butanediamine and after BOC deprotection (M-dots) (red line). Inset: higher magnification of the IR spectra. (C) Dynamic Light Scattering (DLS) measurements of M-dots (100 μg mL^{-1}) showing good solubility in aqueous medium upon functionalization. Inset: digital image of a transparent solution of M-dots (100 μg mL^{-1}). (D) CP MAS ^{29}Si-NMR spectra of unfunctionalized SiO_2 nanoparticles (black line) and M-dots (red line). The presence of an additional band at −86 ppm can be attributed to a SiO_3–N environment confirming the successful functionalization.

measurements showed an average hydrodynamic radius of approximately 290 nm for the M-dots (Fig. 2C) in harmony with the TEM images. Zeta potential (ζ) measurements (in aqueous solution) showed values of -44 ± 2 mV and -26 ± 2 mV for unfunctionalized SiO_2 nanoparticles and M-dots, respectively.[37] In an aqueous medium, M-dots (100 μg mL^{-1}) form a transparent solution showing their improved solubility after surface functionalization (Fig. 2C, inset).

The presence of Si–N surface bonds (due to nucleophilic attack of free amine to a SiO_x–Cl reactive intermediate – $3 > x > 1$) was probed by CP-MAS ^{29}Si-NMR and XPS. The chemical shifts for unfunctionalized SiO_2 nanoparticles were found at -108, -101 and -90 ppm corresponding to well characterized Si environments, *i.e.*, Si bound to four oxygen atoms (Si–O_4 or Q4), surface silanol [Si–O_3 (OH) or Q3] and geminal silanol groups [SiO_2–$(OH)_2$ or Q2], respectively (Fig. 2D, black line).[38,39] However, the CP-MAS ^{29}Si-NMR spectrum of the M-dots (Fig. 2D, red line) displays a lower intensity of the Q4 and Q3 bands compared with unfunctionalized SiO_2 nanoparticles indicating that these environments were partially lost by NH_2 groups during the functionalization process. Additionally, a fourth lower intensity shoulder at *ca.* -86 ppm was observed and can be attributed to a SiO_3–N environment (Fig. 2D, red line).[41]

The Si–N surface chemical bond was further studied by XPS. XPS survey spectra of unfunctionalized SiO_2 nanoparticles show signals with binding energies of 103.3, 151 and 532 eV that were attributed to Si–O_2 (2p), Si–O_2 (2s) and O (1s) respectively (Fig. S2 blue line, ESI†). By comparison, XPS survey spectra of the M-dots show two additional signals at 285.6 eV and a low intensity signal at 405.6 eV that could be assigned to C (1s) and N (1s) (derived from 1,4-butanediamine) suggesting the presence of a Si–N bond and strengthening the idea of amine surface functionalization of the SiO_2 nanoparticles (Fig. S2 orange line, ESI†).

Surprisingly, this functionalization methodology yielded photoluminescent SiO_2 nanoparticles. The M-dots displayed an intrinsic photoluminescence that upon excitation at 380 nm revealed an emission at 430 nm (Fig. 3A, red line). At this excitation wavelength, the unfunctionalized SiO_2 nanoparticles showed no photoluminescence (Fig. 3A, blue dotted line). This photoluminescence can be attributed in part to the existence of surface Si–N bonds as shown by XPS and CP-MAS ^{29}Si-NMR. So far no rational mechanism could be elucidated.[25,27,40,41] However, in survey XPS spectra of the M-dots (Fig. S2, ESI†) no signal was observed at *ca.* 99 eV indicating that no Si centers were generated during the $SOCl_2$ treatment, thus ruling out the possibility of Si centers as the source of the observed intrinsic photoluminescence.

In order to confirm that after amine functionalization the SiO_2 nanoparticles acquire photoluminescence, M-dots (100 μg mL^{-1} in distilled water) were placed onto a glass surface and observed under the CLSM. Fig. 3B shows fluorescent images of M-dots under $\lambda_{ex} = 408$ nm where a blue emission is observed in agreement with the spectral data (Fig. 3A). To demonstrate that this acquired intrinsic photoluminescence is directly related to the nanoparticle functionalization and not a refraction/reflection effect, bleaching experiments of the M-dots were carried out under the CLSM. For this purpose, a defined area of a sample containing M-dots (100 μg mL^{-1} in distilled water) was exposed for 120 s to a higher intensity laser (20% of 30 mW of $\lambda_{ex} = 408$ nm). As a control, another defined area was determined where the laser intensity remained constant, *i.e.*, 4% of 30 mW of $\lambda_{ex} = 408$ nm standard imaging conditions. Fig. 3C shows that the photoluminescence intensity of the M-dots decays when exposed to high laser power (Fig. 3C, black squares), whereas in the control experiments (area irradiated with a lower laser power, $\lambda_{ex} = 408$ nm) it remained relatively stable for 120 s (Fig. 3C, red dots). Thus the high photostability with no blinking and a low degree of photobleaching can be attributed to the M-dots upon excitation at 408 nm. Imaging of the selected area before and after laser irradiation shows complete bleaching of the M-dots confirming their photoluminescence (Fig. 3D).

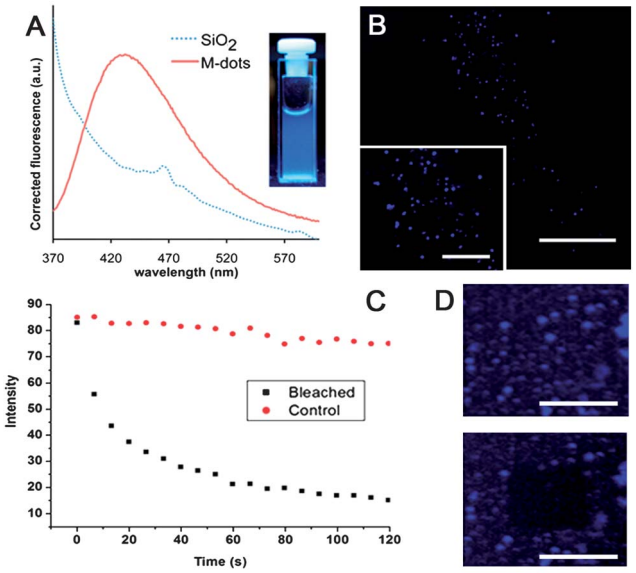

Fig. 3 (A) Photoluminescence spectra of the M-dots (red line) and unfunctionalized SiO_2 nanoparticles (blue dotted line) upon excitation at 380 nm, showing an intense emission band at 430 nm. Inset: digital photograph of a solution of M-dots (100 μg mL^{-1}) under a UV excitation lamp ($\lambda_{ex} = 365$ nm) showing a strong blue photoluminescence. (B) CLSM fluorescence images of M-dots under $\lambda_{ex} = 408$ nm showing strong blue photoluminescence. Inset: higher magnification. Scale bars: 100 and 10 μm respectively. (C) Bleaching experiments. A selected area of the sample was chosen and exposed to a laser intensity of 20% of 30 mW ($\lambda_{ex} = 408$ nm) for 120 s. Where the emission remained stable in control (red circles) the area exposed to higher laser intensity shows a clear decay (black squares) indicating an acquired intrinsic photoluminescence after amine functionalization. (D) Up: imaging of the selected area before exposition to intense laser power. Down: corresponding imaging of the same area after bleaching has taken place. The bleached area can be clearly observed confirming the intrinsic photoluminescence of the M-dots. It is difficult to comment on actual size of the M-dot aggregates based on CLSM because it is below the resolution limit of optical microscopy. Scale bars: 10 μm.

While the quantum yield for the C-dots is (depending on the methodology used for their preparation) within the 10–20% range,[42,43] the quantum yield (ϕ) of the M-dots was determined to be 2.3% (in distilled water, $\lambda_{ex} = 365$ nm).

Given the acquired intrinsic photoluminescence of the M-dots, their biological application has been exploited by studying initially the cytotoxic effect (*e.g.* biocompatibility) exerted in dendritic cells (DCs), and further as a new bioimaging platform

under one- and two-photon excitation. A DC cellular model/nanoparticle interaction (M-dots) was chosen as DCs are relevant for innate and adaptive immune responses and thus may shed light on the *in vivo* behavior of these nanoparticles. The biocompatibility of the M-dots was assessed with a DC viability analysis, *i.e.*, by co-incubating different concentrations of M-dots (50, 100 and 200 μg mL^{-1}) with DCs (Fig. 4A, green bars). A cell viability assay (24 h, 37 °C) revealed that the M-dots were not cytotoxic at any of the concentrations used, *i.e.*, the percentage of cell survival was 114.98 ± 0.3%, 99.91 ± 0.1% and 94.04 ± 0.2%, respectively (Fig. 4A, green bars).

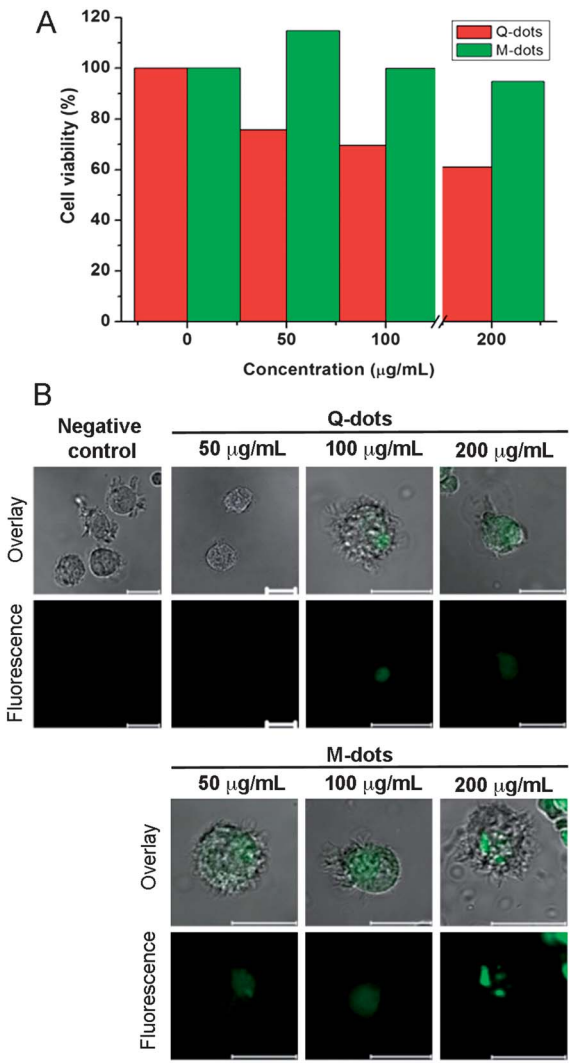

Fig. 4 (A) Cytoxicity of M-dots and PEG-SH capped CdSe/ZnS QDs (comparison) towards DCs at different concentrations (0, 50, 100 and 200 μg mL^{-1}) after co-incubation for 24 h at 37 °C/5% CO_2. No cytotoxicity for the M-dots was observed for any of the concentrations whereas for the CdSe/ZnS QDs a significant decrease in cell viability is observed as function of concentration. (B) CLSM imaging of DCs co-incubated either with Q-dots (upper columns) or M-dots (lower columns) in different concentrations (50, 100 and 200 μg mL^{-1}) for 24 h at 37 °C/5% CO_2. The upper row shows the overlay picture of the DIC-light together with the fluorescence signal. The lower row shows only the emitted fluorescence signal in green (false color) upon λ_{ex} = 408 nm, adjusted to 4% of 30 mW laser power. The instrumental setup was defined so that self-fluorescence of the DCs would not interfere with measurements (negative control). Scale bars: 20 μm.

For comparison, core–shell type quantum dots (QD) (Lumidot™ CdSe/ZnS, λ_{ex} = 475 nm and λ_{em} = 480 nm) were used in parallel. The choice of this type of QD was based on the similarity of the emission wavelengths of the QDs and M-dots. However, the CdSe/ZnS QDs, initially surface stabilized with hexadecylamine (HDA) ligand, were treated in order to become water-soluble by replacing the HDA ligand with PEG-terminated thiol (PEG–SH) (*see Experimental section*).

When different concentrations of PEG–SH capped CdSe/ZnS QDs (50, 100 and 200 μg mL^{-1}) were co-incubated with DCs, a significant concentration-dependent toxicity is observed, *i.e.*, for comparable concentrations, the survival rate of the DCs was significantly lower – 75.82 ± 0.5%, 69.63 ± 0.3% and 61.10 ± 0.7% for 50, 100 and 200 μg mL^{-1}, respectively (Fig. 4A, red bars). These results confirm that the biocompatibility of M-dots is superior to that found for PEG–SH capped CdSe/ZnS QDs as their toxicity has been shown to be associated with ion leaching, which is not possible for the highly condensed SiO_2 contained in the M-dots.

For one-photon imaging, the instrumental background was set up so that the self-fluorescence encountered in DCs (signals derived from shorter lived species) would not interfere with the measurements (Fig. 4B, negative control). After co-incubating M-dots and PEG–SH capped QDs (50, 100 and 200 μg mL^{-1}) with DCs for 24 h at 37 °C/5% CO_2, the cells were imaged. Fig. 4B shows representative microscopic images of one-photon fluorescence (λ_{ex} = 408 nm, adjusted to 4% of 30 mW laser power) (lower row) as well as DIC-Light images overlaid with correspondent one-photon fluorescence images (upper row). Both M-dots and PEG–SH capped QDs can be localized inside the DCs, displaying a comparable fluorescent intensity. It is interesting to note that PEG–SH capped QDs can only be detected inside the cells at concentrations >100 μg mL^{-1}. No uptake occurs at lower concentrations. On the other hand, M-dots are clearly detectable inside DCs at concentrations as low as 50 μg mL^{-1}. The specific uptake mechanism has not been clarified yet.

Further on, the possibility of the M-dots to be two-photon active in aqueous solutions was exploited. A drop of M-dots (100 μg mL^{-1} in distilled water) was placed on a glass surface and imaged using a Zeiss 710 NLO confocal laser scanning microscope (CLSM) equipped with a Coherent femtosecond pulsed Ti:sapphire laser using an excitation wavelength of 753 nm (4% of laser power 305 mW) (among several excitation wavelengths tested, 735 nm yielded the best emission). Fig. 5A and B show that the M-dots emit strong blue and green photoluminescent signals when excited at 753 nm (5% of laser power 305 mW). By recording the two-photon spectrum of M-dots (in aqueous solution) (λ_{ex} = 753 nm) two emission bands at 458 nm and 535 nm are observed, corresponding respectively to the regions of blue and green emission, (Fig. S3, ESI†) in agreement with the imaging data. (Fig. 5A and B) Two-photon photostability of M-dots at λ_{ex} = 753 nm was studied by exposing a selected area of sample to an intense laser radiation (14% of 305 mW) and measuring the intensity variation over 130 s. As control, a different area of the same sample was irradiated with constant laser power (5% of 305 mW) for the same time period.

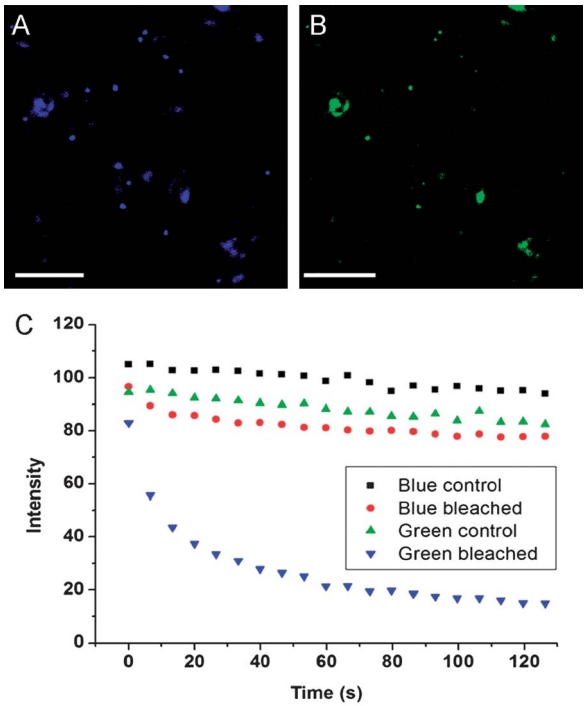

Fig. 5 (A and B) Two-photon images of M-dots acquired under λ_{ex} = 753 nm and laser power of 5% of 305 mW (standard imaging conditions) showing emission in the blue and green regions. Scale bar: 10 μm. (C) Two-photon photostability measurement of blue and green emission regions of M-dots. Selected areas of the samples were exposed to a laser λ_{ex} = 753 nm with 5% of 305 mW laser power (control experiments) and 14% of 305 mW (bleaching experiments) for 130 s. Where the blue emission region remains stable in the control area (black squares) and there is a 20% decrease upon higher laser power exposition (red circles), the green emission region remains stable under standard conditions (control, green triangles) but suffers a strong emission decrease upon higher laser power exposition (blue triangles).

The blue emission remained stable in the control (5% of 305 mW) (Fig. 5C, black squares). On the area that was exposed to higher laser power (14% of 305 mW) an initial intensity decrease of 20% within the first 20 s occurs followed the trend of normal decay observed in the control upon exposition. (Fig. 5C, red circles).

On the other hand, the green emission showed fast intensity decay (50% within the first 20 s) in an area exposed to higher laser power (Fig. 5C, blue triangles) whereas in the control no significant decay (other than the normal trend) was observed. (Fig. 5C, green triangles) The mechanism for these nanoparticles to emit with two-photon excitation is still unknown.

Further bioimaging of cells with two-photon microscopy was carried out (λ_{ex} = 753 nm and 5% of 305 mW). For this purpose, M-dots and PEG–SH capped QDs were co-incubated with DCs at several concentrations (50, 100 and 200 μg mL^{-1}) (24 h, 37 °C/5% CO_2). Again, under these experimental conditions, the instrumental background was set up so that DC auto-fluorescence would not interfere with two-photon measurements (Fig. 6, negative control). Representative images are shown in Fig. 6. The M-dots display a bright blue and green luminescence and an intracellular localization in all concentration ranges used (as observed earlier for one-photon imaging).

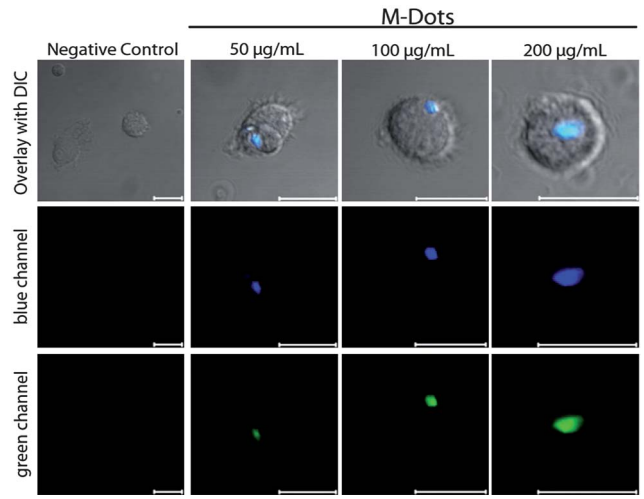

Fig. 6 Two-photon bioimaging of M-dots upon co-incubation with DCs (24 h, 37 °C/5% CO_2) where different concentrations (50, 100, 200 μg mL^{-1}) were used. The instrumental setup was defined so that self-fluorescence of the DCs would not interfere with measurements (negative control). The upper row shows the overlay of the DIC picture with complete fluorescence signals (*e.g.* green and blue). The lower rows show the different fluorescence emitted by the M-dots (blue: 455–500 nm, green: 500–550 nm) when excited by two-photon at λ_{ex} = 753 nm (5% of 305 mW). Scale bars: 20 μm.

Conclusions

In summary, we demonstrated a facile synthetic method to fabricate water stable and dispersible, highly biocompatible and photoluminescent SiO_2 nanoparticles (M-dots) that can easily be conjugated with biomolecules in a single reaction step. The facile biomolecule conjugation together with the extreme robustness of the photophysical properties (one- and two-photon active) make M-dots excellent candidates for biomedical applications ranging from drug delivery to biomolecule labelling (*e.g.* bioimaging). Although C-dots have been considered an alternative to quantum dots (QDs) in biological systems, their applications are less versatile because they are not suitable for biomolecule conjugation as no covalent attachment of the polymer to the inorganic platform exists, and a polymer passivation occurs instead. This passivation can be a strong drawback in biological systems, *i.e.*, during cell internalization the low pH endosomes would promote a detachment of the polymer from the carbon structures resulting in a loss of photoluminescence. On the other hand, C-dots do not allow drug loading and controlled release. The versatility of this methodology can be extended to other SiO_2 based nanosystems, *i.e.*, mesoporous SiO_2 nanoparticles or multifunctional M_xO_y@SiO_2 nanoparticles (M = Fe or Mn) known as MRI contrast agents.

Acknowledgements

This research was supported by the Deutsche Forschungsgemeinschaft through the Priority Program 1313 "Bio-Nano-response". Michael Dietzsch is a recipient of a Carl-Zeiss Fellowship and part of the MAINZ Graduate School for Material Science. We thank Dr Mihail Mondeshki for measuring

the CP MAS ^{29}Si-NMR spectra, the LSM-core facility of the Forschungszentrum Immunologie (FZI) of University of Mainz and to the Center for Complex Matter (COMATT) and the Naturwissenschaftliches Medizinisches Forschungszentrum (NMFZ) at the University of Mainz for support.

References

1 S. Ohkuma and B. Poole, *Proc. Natl. Acad. Sci. U. S. A.*, 1978, **75**, 3327.
2 J. W. Lichtman and J. A. Conchello, *Nat. Methods*, 2005, **2**, 910.
3 M. Chalfie, Y. Tu, G. Euskircher, W. W. Ward and D. C. Prasher, *Science*, 1994, **263**, 802.
4 N. Panchuk-Voloshina, R. P. Haugland, J. Bishop-Stewart, M. K. Bhalgat, P. J. Millard, F. Mao, W.-Y. Leung and R. P. Haugland, *J. Histochem. Cytochem.*, 1999, **47**, 1179.
5 A. P. Alivisatos, W. Gu and C. Larabell, *Annu. Rev. Biomed. Eng.*, 2005, **7**, 55.
6 W. Denk, J. H. Strickler and W. W. Webb, *Science*, 1990, **248**, 73.
7 M. D. Cahalan, I. Parker, S. H. Wei and M. J. Miller, *Nat. Rev. Immunol.*, 2002, **2**, 872.
8 F. Helmchen and W. Denk, *Nat. Methods*, 2003, **21**, 1369.
9 B. Wang and G. K. Halbhuber, *Ann. Anat.*, 2006, **188**, 395.
10 E. M. Sevick-Muraca, J. P. Houston and M. Gurfinkel, *Curr. Opin. Chem. Biol.*, 2002, **6**, 642.
11 D. R. Larson, W. R. Zipfel, R. M. Williams, S. W. Clark, M. P. Bruchez, F. W. Wise and W. W. Webb, *Science*, 2003, **300**, 1434.
12 L. M. Maestro, E. M. Rodriguez, F. S. Rodriguez, M. C. Iglesias-de la Cruz, A. Juarranz, R. Naccache, F. Vetrone, D. Jaque, J. A. Capobianco and J. G. Sole, *Nano Lett.*, 2010, **10**, 5109.
13 M. D. Wissert, B. Rudat, U. Lemmer and H.-J. Eisler, *Phys. Rev. B: Condens. Matter Mater. Phys.*, 2011, **83**, 113304.
14 H. F. Wang, T. B. Huff, D. A. Zweifel, W. He, P. S. Low, A. Wei and J. X. Cheng, *Proc. Natl. Acad. Sci. U. S. A.*, 2005, **102**, 15752.
15 N. J. Durr, T. Larson, D. K. Smith, B. A. Korgel, K. Sokolov and A. Ben-Yakar, *Nano Lett.*, 2007, **7**, 941.
16 A. M. Derfus, W. C. W. Chan and S. N. Bhatia, *Nano Lett.*, 2004, **4**, 11.
17 G. F. Nordberg, *BioMetals*, 2004, **17**, 485.
18 Y. Pan, S. Neuss, A. Leifert, M. Fischler, F. Wen, U. Simon, G. Schmid, W. Brandau and W. Jahnen-Dechent, *Small*, 2007, **3**, 1941.
19 K. B. Male, B. Lachance, S. Hrapovic, G. Sunahara and J. H. T. Luong, *Anal. Chem.*, 2008, **80**, 5487.
20 D.-S. Wang, F.-Y. Hsu and C.-W. Lin, *Opt. Express*, 2009, **17**, 11350.
21 L. Cao, X. Wang, M. J. Meziani, F. Lu, H. Wang, P. G. Luo, Y. Lin, B. A. Harruff, L. M. Veca, D. Murray, S.-Y. Xie and Y.-P. Sun, *J. Am. Chem. Soc.*, 2007, **129**, 11318.
22 C. Tu, X. Ma, P. Pantazis, S. M. Kauzlarich and A. Y. Louie, *J. Am. Chem. Soc.*, 2010, **132**, 2016.
23 S. A. Hilderbrand, F. Shao, C. Salthouse, U. Mahmood and R. Weissleder, *Chem. Commun.*, 2009, 4188.
24 M. Wang, C.-C. Mi., W.-X. Wang, C.-H. Liu, Y.-F. Wu, Z.-R. Xu, C.-B. Mao and S.-K. Xu, *ACS Nano*, 2009, **3**, 1580.
25 W. H. Green, K. P. Le, J. Grey, T. T. Au and M. J. Sailor, *Science*, 1997, **276**, 1826.
26 A. M. Jakob and T. A. Schmedake, *Chem. Mater.*, 2006, **18**, 3173.
27 L. Wang, M. C. Estévez, M. O'Donoghue and W. Tan, *Langmuir*, 2008, **24**, 1635.
28 F. Enrichi, E. Trave and M. Bersani, *J. Fluoresc.*, 2008, **2**, 507.
29 R. B. Soriano, E. Kpatcha, A. M. Jakob, J. W. Merkert, C. M. Carlin and T. A. Schmedake, *Appl. Phys. Lett.*, 2007, **91**, 091909.
30 S. Kohli, J. A. Theil, P. C. Dippo, K. M. Jones, M. M. Al-Jassim, R. K. Ahrenkiel, C. D. Rithner and P. K. Dorhout, *Nanotechnology*, 2004, **15**, 1831.
31 N. Daldosso, G. Das, S. Larcheri, G. Mariotto, G. Dalba, L. Pavesi, A. Irrera, F. Priolo, F. Iacona and F. Rocca, *J. Appl. Phys.*, 2007, **101**, 113510.
32 J. E. Riggs, Z. Guo, D. L. Carroll and Y.-P. Sun, *J. Am. Chem. Soc.*, 2000, **122**, 5879.
33 D. M. Shendage, R. Froehlich and G. Haufe, *Org. Lett.*, 2004, **6**, 3675.
34 J. R. Lakowicz, in *Principles of Fluorescence Spectroscopy*, Kluwer Academic/Plenum Publisher, New York, 2nd edn, 1999.
35 S. J. Lang and B. A. Morrow, *J. Phys. Chem.*, 1994, **98**, 13314.
36 R. J. P. Corriu, D. Leclercq, P. H. Mutin, J. M. Planeix and A. Vioux, *J. Organomet. Chem.*, 1991, **406**, C1.
37 R. P. Bagwe, L. R. Hilliard and W. Tan, *Langmuir*, 2006, **22**, 4357.
38 R. van Weeren, E. A. Leone, S. Curran, L. C. Klein and S. C. Danforth, *J. Am. Ceram. Soc.*, 1994, **77**, 2699.
39 Y. Xia and R. Mokaya, *J. Mater. Chem.*, 2004, **14**, 2507.
40 K. J. Price, L. R. Sharpe, L. E. McNeil and E. A. Irene, *J. Appl. Phys.*, 1999, **86**, 2638.
41 M. Ueda, H. Reuther, A. F. Beloto, C. Kuranaga and E. Abramof, *IEEE Trans. Plasma Sci.*, 2006, **34**, 1080.
42 Y.-P. Sun, B. Zhou, Y. Lin, W. Wang, K. A. S. Fernando, P. Pathak, M. J. Meziani, B. A. Harruff, X. Wang, H. F. Wang, P. J. G. Luo, H. Yang, M. E. Kose, B. L. Chen, L. M. Veca and S. Y. Xie, *J. Am. Chem. Soc.*, 2006, **128**, 7756.
43 S.-T. Yang, L. Cao, P. G. Luo, F. Lu, X. Wang, H. Wang, M. J. Meziani, Y. Liu, G. Qi and Y.-P. Sun, *J. Am. Chem. Soc.*, 2009, **131**, 11308.

